nature materials

LETTERS

PUBLISHED ONLINE: 23 MARCH 2015 | DOI: 10.1038/NMAT4250

Hybrid optical–electrical detection of donor electron spins with bound excitons in silicon

C. C. Lo[1,2]*, M. Urdampilleta[1], P. Ross[1], M. F. Gonzalez-Zalba[3], J. Mansir[1], S. A. Lyon[4], M. L. W. Thewalt[5] and J. J. L. Morton[1,2]

Electrical detection of spins is an essential tool for understanding the dynamics of spins, with applications ranging from optoelectronics[1,2] and spintronics[3], to quantum information processing[4–8]. For electron spins bound to donors in silicon, bulk electrically detected magnetic resonance has relied on coupling to spin readout partners such as paramagnetic defects[4,5] or conduction electrons[6–8], which fundamentally limits spin coherence times. Here we demonstrate electrical detection of donor electron spin resonance in an ensemble by transport through a silicon device, using optically driven donor-bound exciton transitions[9,10]. We measure electron spin Rabi oscillations, and obtain long electron spin coherence times, limited only by the donor concentration[11]. We also experimentally address critical issues such as non-resonant excitation, strain, and electric fields, laying the foundations for realizing a single-spin readout method with relaxed magnetic field and temperature requirements compared with spin-dependent tunnelling[12,13], enabling donor-based technologies such as quantum sensing.

Shallow donor electron and nuclear spins in silicon have extraordinarily long coherence times[9–11], making them attractive candidates for quantum information processing[14], quantum memory[15], as well as for quantum sensing applications[16]. In addition, neutral shallow donors can form bound exciton states (D^0X) with relatively long lifetimes (∼200–300 ns; ref. 17) and correspondingly narrow intrinsic linewidths, enabling optical transitions with both electron and nuclear spin selectivity[18]. D^0X can be formed by a direct photon excitation (a no-phonon transition) with energy $E[D^0X] \sim 1.15$ eV, just below the silicon indirect bandgap of $E_g = 1.17$ eV. The photon excites an electron from the valence band at the neutral donor site, resulting in two indistinguishable electrons and one hole localized in the D^0X ground state. The D^0X state then relaxes via an Auger recombination process where the excess electron–hole pair recombines and its energy is transferred to the remaining electron, ejecting it from the donor site and leaving behind the positively charged donor ion.

The D^0X spin-selective optical transitions are attractive for realizing hybrid optical–electrical ensemble spin detection in silicon as no decoherence-inducing paramagnetic centre close to the dopant is required for spin-charge conversion. In addition, they could enable high-fidelity single-dopant electron spin readout without the requirement of keeping the thermal energy much less than the Zeeman splitting—this is in contrast with spin-dependent tunnelling schemes[12], where, for example, ∼80% electron spin readout fidelity was achieved at $T \sim 300$ mK and $B \sim 1$ T (ref. 13).

The maximum temperature for spin readout using D^0X is limited by its dissociation energy of approximately 5 meV (ref. 19), such that this could be readily implemented at liquid helium temperatures—our experiments were carried out at 4.3 K (see Supplementary Section I for the temperature dependence of the bound exciton spectrum). Spin readout fidelity is instead determined by the optical transition linewidths (approximately 20 neV when lifetime limited) compared to the D^0X spin splitting, which is always at least the hyperfine interaction strength ($A = 0.486$ µeV for phosphorus donors, ^{31}P). Hence, zero-magnetic-field measurements are possible in principle. These strongly relaxed experimental conditions open the possibility of practical implementation of quantum sensing applications with donor spins[16], and enable access to the long donor spin relaxation times observed at low magnetic fields ($B \ll 1$ T; ref. 11).

The D^0X Auger recombination process has recently been used in conjunction with contact-less capacitive schemes in bulk silicon for the detection of nuclear spin coherence times in highly enriched ^{28}Si (refs 9,10). We apply this technique for electrical detection of D^0X spectroscopy via direct transport measurements through devices built on epitaxially grown ^{28}Si doped with ^{31}P at 10^{15} cm^{-3} (Fig. 1). The ^{28}Si epitaxial layer has a built-in biaxial strain due to its lattice mismatch with the undoped substrate of natural isotope abundance[20]. The presence of strain modifies the local bandgap surrounding the donors by lifting the degeneracy of the valence and conduction band edges, and consequently shifts the donor binding energies through valley repopulation[21]. The states undergo further Zeeman splitting in an applied magnetic field, leading to six pairs of dipole-allowed transitions ($\Delta m = 0, \pm 1$), which we observe by monitoring the current through the device as the laser wavelength is swept. Owing to the strain distribution in the epitaxial material and local strains induced by the electrical contacts, we do not resolve the hyperfine splitting of the ^{31}P donors in this silicon device. By mapping out the magnetic field dependence of the D^0X spectrum we obtain a complete picture of the valence band light hole (LH), heavy hole (HH) and Zeeman splittings, where the measured zero-field splitting $\Delta E_{VB} = 19$ µeV is due to the $\epsilon_{\parallel} = +2.4 \times 10^{-6}$ (tensile) biaxial strain-induced LH–HH splitting. Assuming an isotropic g-factor of $g_d = 1.9985$ for the ^{31}P donor electrons[22], we find the D^0X hole-state g-factors to be $g_{LH} = 0.86$ and $g_{HH} = 1.33$ in this magnetic field orientation ($B \parallel \langle 100 \rangle$), in good agreement with earlier measurements (see Supplementary Section II). Our device geometry allows us to study the effect of the LH–HH splitting as a function of electric field (Fig. 1e), yielding a linear Stark shift parameter of $2p_8 = 33 \pm 7$ µeV (V/µm)$^{-1}$, or $p_8 = 0.8$ D, similar to

[1]London Centre for Nanotechnology, University College London, London WC1H 0AH, UK. [2]Department of Electronic and Electrical Engineering, University College London, London WC1E 7JE, UK. [3]Hitachi Cambridge Laboratory, J. J. Thomson Avenue, Cambridge CB3 0HE, UK. [4]Department of Electrical Engineering, Princeton University, Princeton, New Jersey 08544, USA. [5]Simon Fraser University, Burnaby, British Columbia V5A 1S6, Canada.
*e-mail: cheuk.lo@ucl.ac.uk

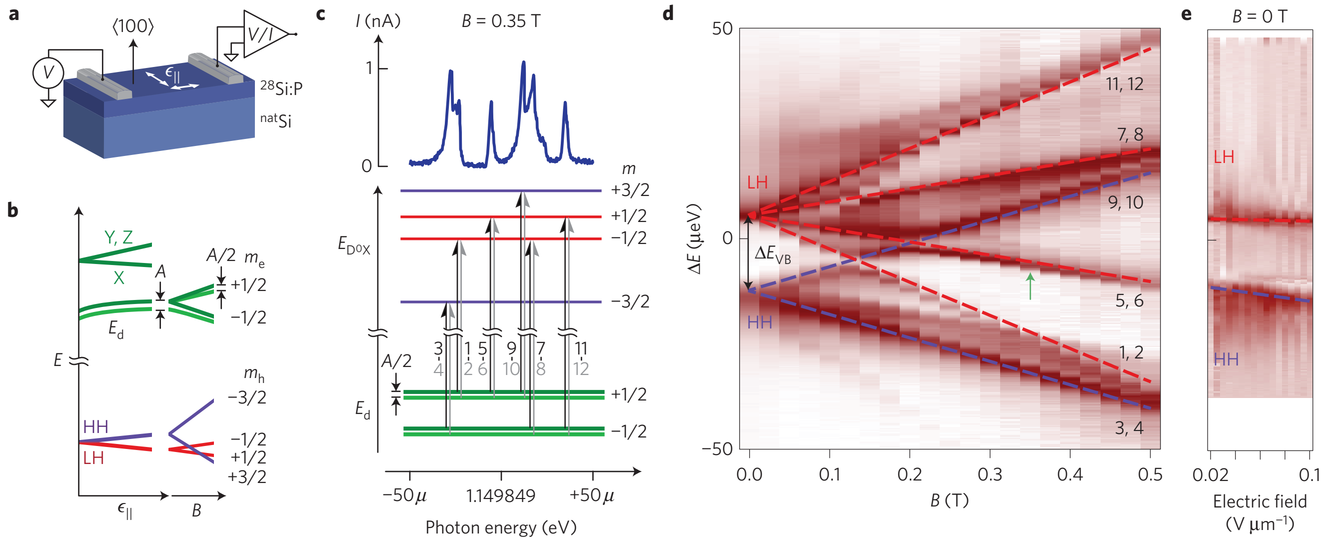

Figure 1 | Electrically detected D^0X spectroscopy in a silicon device. a, Schematic of the ^{31}P-doped ^{28}Si epitaxial layer (with in-plane strain $\epsilon_{||}$) on an undoped natural Si substrate. **b**, Energy shifts of the conduction band valleys (X, Y and Z), donor (E_d), and light hole (LH) and heavy hole (HH) valence bands due to $\epsilon_{||}$ and magnetic field B. **c**, Allowed transitions for D^0X formation at $B = 0.35$ T (labelled according to convention; ref. 9) and the measured spectrum. **d**, B dependence of the spectrum, with dashed lines showing fits based on the extracted g-factors and $\epsilon_{||}$. The green arrow indicates the optical transition used in subsequent measurements. **e**, Electric field dependence of D^0X spectrum at $B = 0$ T shows the Stark shifts of the LH and HH bands. Dashed lines are linear fits to the LH and HH peak positions.

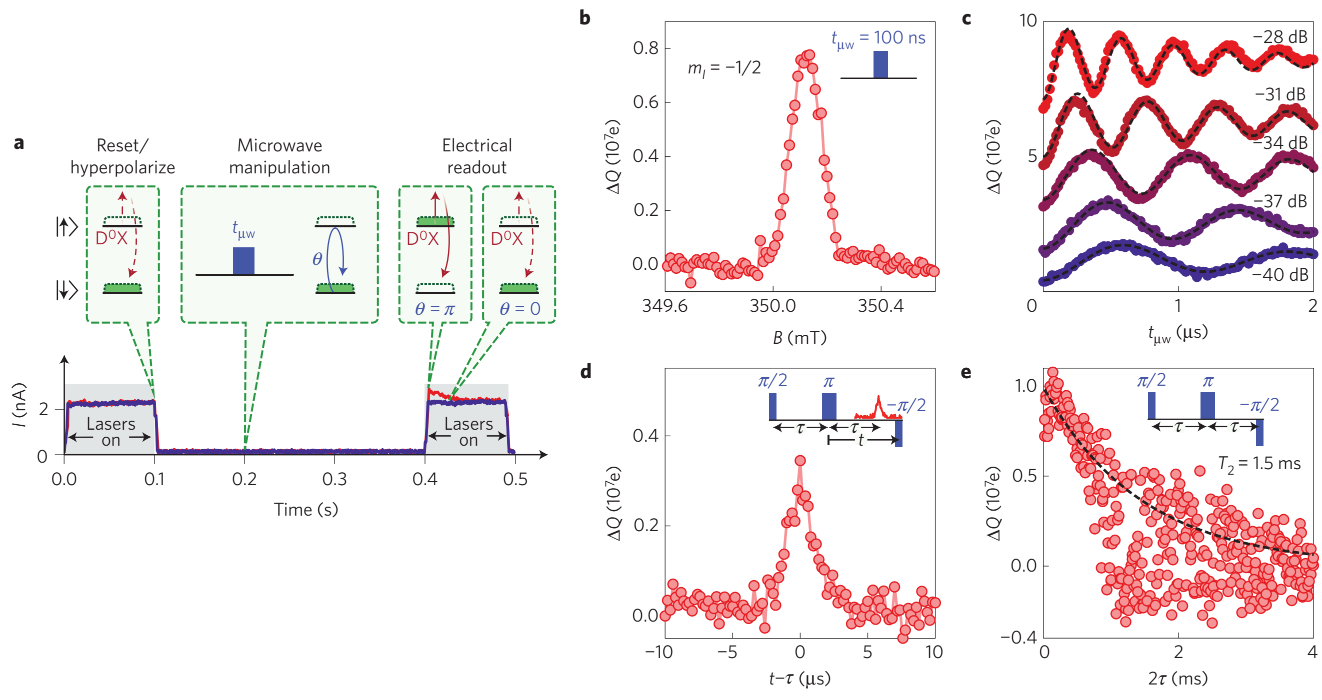

Figure 2 | Electrically detected spin resonance using D^0X. a, The initial laser pulse hyperpolarizes the electron spins into the $|\downarrow\rangle$ state, and is followed by a microwave pulse of duration $t_{\mu w}$ corresponding to some rotation θ ($\theta = 0$, purple trace, or $\theta = \pi$, red trace). The current transient during the 'readout' laser pulse is used to measure the electron spin population in the $|\uparrow\rangle$ state. **b**, Magnetic field sweep with a fixed $t_{\mu w} = 100$ ns microwave pulse, where the ^{31}P ESR transition with $m_I = -1/2$ is detected. **c–e**, Coherent control and electrical detection of the donor state demonstrated by Rabi oscillations (the microwave power attenuations are as indicated and the traces are offset for clarity) (**c**), Hahn echo signal for $\tau = 20\,\mu$s (**d**), and T_2 measurement (**e**). Dashed lines are fits to the experimental data.

acceptor states in silicon[23]. Carrier injection from the electrical contacts prohibits measurements at larger electric fields.

To demonstrate electrical detection of electron spin resonance using D^0X we set the magnetic field to $B \sim 0.35$ T and tune our laser on resonance with transitions 5–6, as shown in Fig. 1d. This optical excitation drives the spin-selective ionization of spin-up electrons, after some time (~100 ms) leaving the donor electrons hyperpolarized into the spin-down state[18]. The laser excitation is turned off to allow coherent control of the donor spins via applied microwave pulses, and then turned on again for readout. Figure 2a shows the measured current transients with, and without, a microwave π pulse applied, illustrating how the difference in the

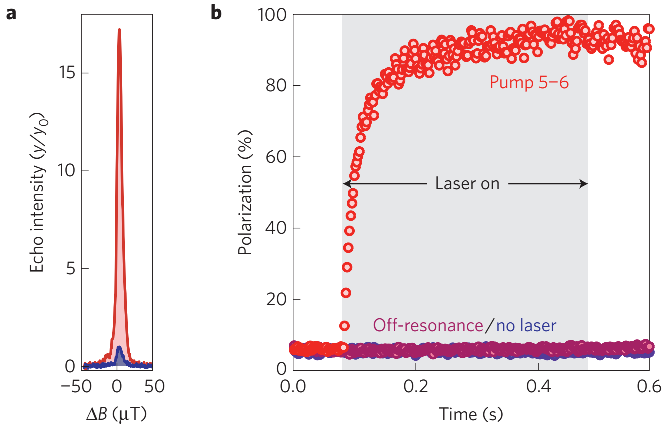

Figure 3 | ESR detection under D^{0}X laser excitation. a, Electron spin echo-detected field sweep of the $m_I = -1/2$ hyperfine line of ^{31}P donors in a ^{28}Si crystal, measured at 4.3 K in thermal equilibrium (blue), and with the laser tuned to transitions 5–6 (red), showing a signal enhancement by a factor of ~18. **b**, The dynamics of the hyperpolarization process is studied with the D^{0}X laser tuned to transitions 5–6 (red), tuned off resonance by 3 µeV (purple), and measured with the laser turned off completely (blue). The lack of response when the laser is off resonance indicates non-resonant ionization processes are negligible here.

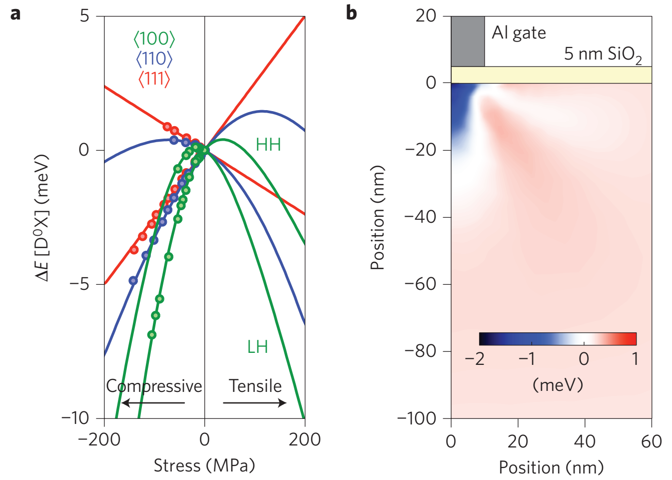

Figure 4 | Strain-induced shifts in D^{0}X transition energies, ΔE[D^{0}X]. a, Uniaxial stress applied along the major crystallographic directions: ⟨100⟩, ⟨110⟩ and ⟨111⟩. The lines are results from our calculation, and circles are data taken from ref. 30. **b**, Calculated ΔE[D^{0}X] due to thermal expansion coefficient mismatch for ^{31}P donors in close proximity to aluminium electrodes and under a 5 nm gate oxide at 4.2 K. Only the higher energy of the two strain-induced valence band branches for the transitions are shown. See Supplementary Information for details.

integrated signals between the two is a measure of the donor spin z-projection. With a microwave pulse of fixed duration $t_{\mu w} = 100$ ns, we first perform a magnetic field sweep to confirm that the laser-induced current transients arise from the ^{31}P donors (Fig. 2b). The observed ESR linewidth is ~200 µT (or about 0.6 MHz, owing to the microwave pulse bandwidth), which means that, even though the hyperfine splitting (117 MHz) is not optically resolved in our device, it can be readily resolved by ESR and this technique can be extended to perform electrical detection of electron–nuclear spin double resonance[24]. Next, with the magnetic field fixed at the $m_I = -1/2$ resonance transition, we measure electron spin Rabi oscillations by varying the duration of the microwave pulse (Fig. 2c), demonstrating coherent manipulation and electrical detection of the donor spin states and yielding an ensemble dephasing time of $T_2^* = 2$ µs caused by the strain distribution in the sample.

We measure the electron spin coherence time by implementing a two-pulse Hahn echo sequence with an additional 'readout' $\pi/2$ pulse to project the coherence into the population of the spin eigenstate. An example Hahn echo is shown in Fig. 2d and the echo decay is plotted in Fig. 2e. The fluctuations in signal amplitude after 1 ms are due to the presence of instrumental magnetic field noise so that only the period $2\tau \le 1$ ms was fitted to extract the spin coherence time. The measured value of $T_2 = 1.5$ ms is in good agreement with bulk spin resonance measurements for samples under similar dopant concentrations, isotopic purity, temperature and magnetic field[11]. This reflects an inherent advantage of using spin-selective optical transitions for electrical readout, as the donor spin coherence is no longer inherently limited by nearby sources of decoherence, where, for instance, $T_2 \sim 1$ µs for spin-dependent recombination with interface paramagnetic defects[5].

To apply this approach in single-donor qubit and quantum sensing applications, two crucial factors impacting electron spin readout fidelity are the ability to detect the resonantly formed ionized donor state (for example, using a charge sensor for single donors), and avoid false readings arising from non-resonant ionization events. The former is unlikely to be limiting, as bound excitons can be resonantly generated at a much faster rate (~85 MHz in our experimental set-up, see Supplementary Section III) than typical spin relaxation times ($T_1 \sim 100$ s; ref. 11). Once ionized, the dopant neutralization time is of the order of 10 ms (depending strongly on the abundance of free carriers in the vicinity of the dopant), which is ample for charge state detection. On the other hand, non-resonant ionization of the donor state can be caused by off-resonance photons directly ionizing neutral donors, or creating free excitons which subsequently recombine at neutral donor sites (we note, however, the energy required for free exciton formation is approximately 5 meV higher than resonant D^{0}X transitions in bulk silicon). As no spin resonance signal can be observed with electrical detection when the D^{0}X laser is tuned off resonance, we examine the role of non-resonant irradiation in more detail below by observing its effect on bulk electron spin resonance (ESR) measurements.

We first show the effect of the D^{0}X laser (tuned to the 5–6 transition as before) on the ESR signal, as observed in an echo-detected field sweep (Fig. 3a). The echo signal amplitude is greatly enhanced owing to hyperpolarization of the electron spins (see Supplementary Section IV), and the dynamics of this process can be seen through the change in echo intensity at different times during the laser pulsing sequence, as shown in Fig. 3b. When the laser is detuned from resonance by 3 µeV, the echo intensity remains constant and identical to the thermal equilibrium measurement. This demonstrates that off-resonant ionization is negligible in dilutely doped substrates, as both direct ionization and free exciton–donor recombination would diminish the echo intensity. Nevertheless, if non-resonant ionization is found to affect readout fidelity to some degree, the donor nuclear spin could be used as an ancilla for performing repetitive measurements[25].

Below we address further considerations for extending these results to realize practical single-donor devices using neutral donor-bound excitons, in particular the effects of strain and electric fields in nanodevices. As observed in our silicon device, the D^{0}X transition energies are extremely sensitive to the presence of local strains. Figure 4a shows the calculated change in D^{0}X transition energies, ΔE[D^{0}X], for ^{31}P donors at zero magnetic field for uniaxial stresses up to 200 MPa (~10^{-3} strain; see Supplementary Section V), which are not uncommon in silicon nanodevices[26]. The calculated ΔE[D^{0}X] for a conventional donor device architecture due to thermal expansion coefficient mismatching of the silicon substrate, gate dielectric and aluminium gate electrodes[26] is illustrated in

Fig. 4b. The uncertainty in dopant positioning in the device can cause a large detuning of the transition energies, which are orders of magnitude greater than the spin splitting. Although the transition energies can always be calibrated for individual single-donor devices, a large inhomogeneous strain distribution in multi-donor device architectures would make spin detection by D^0X impractical. We note that this sensitivity to strain is more severe for D^0X than for optical transitions of erbium ions in silicon[27], where only core shell electronic levels are involved.

The electric fields present in silicon nanodevices will also shift the D^0X energy, as we have already shown above through the Stark splitting of the hole states. However, if the field is particularly strong, it is expected to further reduce the bound exciton lifetime in an analogous process to field ionization of donors, but taking into account the much lower binding D^0X energy of 5 meV. Therefore, both strain and electric fields in realistic single-dopant devices must be carefully considered and controlled for the successful implementation of D^0X-based spin readout.

A hybrid optical–electrical single-donor detection scheme using donor-bound excitons coupled to a quantum point contact has been previously proposed[28]; however, the uncertainty in local strain and relatively large electric fields present in metal–oxide–semiconductor-based architectures will make measuring bound excitons difficult. Although D^0X detection can conversely be used as an extremely sensitive probe to quantify strain and electric fields of silicon nanostructures and devices on the atomistic scale, reducing these perturbative field distributions will be crucial for implementing hybrid optical–electrical detection for large arrays of qubit devices on a single chip. Therefore, an optimally designed readout device should have both the strain and electric fields carefully controlled (and minimized) in the vicinity of the dopant. For instance, epitaxially grown[29] or nanowire single-electron transistors operating at liquid helium temperatures can be used as the charge detector, and in this hybrid spin detection scheme the need for dilution refrigerators can be completely alleviated, opening the door to the exploitation of ultra-long coherent donor spins for practical quantum technological applications.

Methods

Samples and preparation. The electrical detection of D^0X spectroscopy and spin resonance was performed on a ^{31}P-doped (10^{15} cm^{-3}) 25 µm thick ^{28}Si (99.9%) layer, epitaxially grown on a nominally undoped natural silicon substrate. Electron beam lithography was used to pattern electrodes 20 µm wide and 700 µm in length, and with a 100 µm gap. A total of $\sim 10^9$ donors are probed in the electrical detection given the device geometry. 30 nm of aluminium was subsequently evaporated and lifted off, forming the electrical contacts of the device. The sample used for the bulk electron spin resonance measurements was a ^{31}P-doped (10^{14} cm^{-3}) isotopically enriched 99.995% ^{28}Si crystal with dimensions of approximately $2 \times 2 \times 10$ mm^3.

D^0X spectroscopy and electron spin resonance. All experiments were carried out using an Oxford Instruments CF 935 optical cryostat operating at $T = 4.3$ K. For D^0X spectroscopy with magnetic field sweeps (Fig. 1d), a lock-in detection was used to measure the change in sample impedance as the D^0X laser was scanned, and the normalized change in signal phase was recorded. For electric field sweeps (Fig. 1e), an arbitrary waveform generator (Agilent 33522A) was used to generate short (300 µs) voltage pulses to minimize any heating effects caused by electrical currents. A low-noise current amplifier (Femto DLPCA) was used to amplify and measure the electrical current, and the transients were captured on a digital oscilloscope (Agilent MSO-X 3104A). Pulsed microwaves were controlled by an X-band Bruker Elexsys 580E pulsed ESR spectrometer with a 1 kW travelling-wave tube microwave amplifier, operating at the resonator frequency of 9.7 GHz. For electrical detection of spin resonance, d.c. biasing was provided by a low-noise voltage source (Stanford Research SIM915).

Optical set-up. A Koheras Boostik fibre laser (NKT Photonics) was used for bound exciton formation (D^0X laser), with an optical linewidth of approximately 70 kHz. The fibre laser input power was approximately 3 mW mm^{-2} into the cryostat window and resonator. A 2 nm bandpass filter centred at around 1,078 nm was used to suppress any spurious outputs from the fibre laser. For the electrical readout of spin resonance experiments, an above-bandgap laser at 1,047 nm was set to approximately 1 mW mm^{-2}, and synchronized with the D^0X laser to facilitate donor neutralization and reduction of electrical current drift. For the experiments with direct ESR detection of bulk-doped silicon, the above-bandgap laser was set to approximately 50 mW mm^{-2}, and was used only at the beginning of each measurement cycle to reset the spin polarization to thermal equilibrium (and not used for the remainder of the measurement sequence). The laser spot sizes were approximately 2 mm.

Received 5 November 2014; accepted 12 February 2015; published online 23 March 2015

References

1. Malissa, H. *et al.* Room-temperature coupling between electrical current and nuclear spins in OLEDs. *Science* **345,** 1487–1490 (2014).
2. Algasinger, M. *et al.* Improved black silicon for photovoltaic applications. *Adv. Energy Mater.* **3,** 1068–1074 (2013).
3. Appelbaum, I., Huang, B. & Monsma, D. J. Electronic measurements and control of spin transport in silicon. *Nature* **447,** 295–298 (2007).
4. Stegner, A. R. *et al.* Electrical detection of coherent ^{31}P spin quantum states. *Nature Phys.* **2,** 835–838 (2006).
5. Paik, S. Y., Lee, S. Y., Baker, W. J., McCamey, D. R. & Boehme, C. T_1 and T_2 spin relaxation time limitations of phosphorus donor electron near crystalline silicon to silicon dioxide interface defects. *Phys. Rev. B* **81,** 075214 (2010).
6. McCamey, D. R., van Tol, J., Morley, G. W. & Boehme, C. Electronic spin storage in an electrically readable nuclear spin memory with a lifetime >100 seconds. *Science* **330,** 1652–1656 (2010).
7. Lo, C. C. *et al.* Electrically detected magnetic resonance of neutral donors interacting with a two-dimensional electron gas. *Phys. Rev. Lett.* **106,** 207601 (2011).
8. Lo, C. C., Weis, C. D., van Tol, J., Bokor, J. & Schenkel, T. All-electrical nuclear spin polarization of donors in silicon. *Phys. Rev. Lett.* **110,** 057601 (2013).
9. Steger, M. *et al.* Quantum information storage for over 180s using donor spins in a ^{28}Si "semiconductor vacuum". *Science* **336,** 1280–1283 (2012).
10. Saeedi, K. *et al.* Room-temperature qubit storage exceeding 39 minutes using ionized donors in ^{28}Si. *Science* **342,** 830–833 (2013).
11. Tyryshkin, A. M. *et al.* Electron spin coherence exceeding seconds in high-purity silicon. *Nature Mater.* **11,** 143–147 (2012).
12. Morello, A. *et al.* Single-shot readout of an electron spin in silicon. *Nature* **467,** 687–691 (2010).
13. Pla, J. J. *et al.* A single-atom electron spin qubit in silicon. *Nature* **489,** 541–545 (2012).
14. Kane, B. A silicon-based nuclear spin quantum computer. *Nature* **393,** 133–137 (1998).
15. Morton, J. J. L. *et al.* Solid-state quantum memory using the ^{31}P nuclear spin. *Nature* **455,** 1085–1088 (2008).
16. Taylor, J. *et al.* High-sensitivity diamond magnetometer with nanoscale resolution. *Nature Phys.* **4,** 810–816 (2008).
17. Schmid, W. Auger lifetimes for excitons bound to neutral donors and acceptors in Si. *Phys. Status Solidi B* **84,** 529–540 (1977).
18. Yang, A. *et al.* Simultaneous sub second hyper polarization of the nuclear and electron spins of phosphorus in silicon by optical pumping of exciton transitions. *Phys. Rev. Lett.* **102,** 257401 (2009).
19. Haynes, J. R. Experimental proof of the existence of a new electronic complex in silicon. *Phys. Rev. Lett.* **4,** 361 (1960).
20. Yang, A. *et al.* High-resolution photoluminescence measurement of the isotopic-mass dependence of the lattice parameter of silicon. *Phys. Rev. B* **77,** 113203 (2008).
21. Wilson, D. K. & Feher, G. Electron spin resonance experiments on donors in silicon. III. Investigation of excited states by the application of uniaxial stress and their importance in relaxation processes. *Phys. Rev.* **124,** 1068–1083 (1961).
22. Feher, G. Electron spin resonance experiments on donors in silicon. I. Electronic structure of donors by electron nuclear double resonance technique. *Phys. Rev.* **114,** 1219–1244 (1959).
23. Kopf, A. & Lassmann, K. Linear Stark and nonlinear Zeeman coupling to the ground state of effective mass acceptors in silicon. *Phys. Rev. Lett.* **69,** 1580–1583 (1992).
24. Hoehne, F., Dreher, L., Huebl, H., Stutzmann, M. & Brandt, M. S. Electrical detection of coherent nuclear spin oscillations in phosphorus-doped silicon using pulsed endor. *Phys. Rev. Lett.* **106,** 187601 (2011).
25. Jiang, L. *et al.* Repetitive readout of a single electronic spin via quantum logic with nuclear spin ancillae. *Science* **326,** 267–272 (2009).
26. Thorbeck, T. & Zimmerman, N. M. Formation of strain-induced quantum dots in gated semiconductor nanostructures. Preprint at http://arxiv.org/abs/1409.3549 (2014).

27. Yin, C. *et al.* Optical addressing of an individual erbium ion in silicon. *Nature* **497,** 91–95 (2013).
28. Sleiter, D. *et al.* Quantum hall charge sensor for single-donor nuclear spin detection in silicon. *New J. Phys.* **12,** 093028 (2010).
29. Fuhrer, A., Füchsle, M., Reusch, T. C. G., Weber, B. & Simmons, M. Y. Atomic-scale, all epitaxial in-plane gated donor quantum dot in silicon. *Nano Lett.* **9,** 707–710 (2009).
30. Thewalt, M. L. W. & Rostworowski, J. A. Effects of uniaxial stress on the luminescence lines due to multiexciton complexes bound to phosphorus in silicon. *Phys. Rev. Lett.* **41,** 808–812 (1978).

Acknowledgements

We thank A. M. Tyryshkin for useful discussions. This research is supported by the EPSRC through the Materials World Network (EP/I035536/1) and UNDEDD project (EP/K025945/1) as well as by the European Research Council under the European Community's Seventh Framework Programme (FP7/2007-2013) through grant agreements No. 279781 (ERC) and 318397. Work at Princeton is supported by NSF through Materials World Network (DMR-1107606) and through the Princeton MRSEC (DMR-01420541). C.C.L. is supported by the Royal Commission for the Exhibition of 1851. J.J.L.M. is supported by the Royal Society.

Author contributions

C.C.L., M.U., M.F.G-Z. and J.J.L.M. conceived and designed the experiments. M.L.W.T. and S.A.L. provided the silicon samples. M.U. fabricated the silicon device, and the experiments were carried out by C.C.L., M.U. and P.R. C.C.L. developed the strain model for D^0X and J.M. performed the strain simulations. All authors discussed the results. C.C.L. and J.J.L.M. wrote the manuscript with input from all authors.

Additional information

Supplementary information is available in the online version of the paper. Reprints and permissions information is available online at www.nature.com/reprints. Correspondence and requests for materials should be addressed to C.C.L.

Competing financial interests

The authors declare no competing financial interests.